energies

MDPI

Article

Decay on Cyclic CO_2 Capture Performance of Calcium-Based Sorbents Derived from Wasted Precursors in Multicycles

Dehong Gong [1,2], Zhongxiao Zhang [1,*] and Ting Zhao [2]

[1] School of Energy and Power Engineering, University of Shanghai for Science and Technology, Shanghai 200093, China; gdh191@163.com
[2] School of Electrical Engineering, Guizhou University, Guiyang 550025, China; tzhao@gzu.edu.cn
* Correspondence: zhzhx222@163.com; Tel.: +86-13501618961

Abstract: In order to obtain the cheap waste calcium-based sorbent, three wasted $CaCO_3$ precursors, namely carbide slag, chicken eggshells, and analytical reagent-grade calcium carbonate, were selected and prepared at 700 °C to form calcium-based sorbents for CO_2 capture. TGA was used to test the CO_2 uptake performance of each calcium-based sorbent in 20 cycles. To identify the decay mechanism of CO_2 uptake with an increasing number of cycles, all calcium-based sorbents were characterized by using XRF, XRD, and N_2 adsorption. The specific surface area of calcium-based sorbents was used to redefine the formula of cyclic carbonation reactivity decay. The carbonation conversion rate of three calcium-based sorbents exhibited a decreasing trend as the cycle number increased. Chicken eggshells exhibited the most significant decrease rate (over 50% compared with Cycle 1), while carbide slag and analytical reagent-grade calcium carbonate showed a flat linear decline trend. The specific surface area of the samples was used to calculate carbonation conversion for an infinite number of cycles. The carbonation conversion rates of three calcium-based sorbents were estimated to decrease to 0.2898, 0.1455, and 0.3438 mol/mol, respectively, after 100 cycles.

Keywords: carbon dioxide capture; carbonation reaction; thermogravimetric analysis; calcium looping

Citation: Gong, D.; Zhang, Z.; Zhao, T. Decay on Cyclic CO_2 Capture Performance of Calcium-Based Sorbents Derived from Wasted Precursors in Multicycles. *Energies* **2022**, *15*, 3335. https://doi.org/10.3390/en15093335

Academic Editor: João Fernando Pereira Gomes

Received: 12 April 2022
Accepted: 2 May 2022
Published: 3 May 2022

1. Introduction

Anthropogenic climate change, which is caused by a large number of greenhouse gas emissions, especially the emission of CO_2, is becoming a focus and severe challenge for many countries in the world [1]. According to their own national conditions, many countries have set up their own targets of carbon peak carbon neutralization by the end of 2060 or 2050 [2]. Reducing the cosumption of fossil fuels and promoting the application of CCUS (Carbon Capture, Utilization and Storage) are the most important technical measures for achieving the target of carbon neutralization on the premise of ensuring national energy security. Untill now, the fossil fuel power plants are still the primary contributor to anthropogenic CO_2 emissions, which accounted for more than 33% of global CO_2 emissions. Even the hydrogen energy, a promising alternative energy source, is still mainly produced from fossil fuels [3–5]. As a result, it will become more and more important to further develop high-efficiency, low-cost and large-scale CCUS technology in the near future, especially for China, which is the country with the most coal-dominant energy structure [6–8].

There are many CCUS technologies, such as the membrane separation method, the chemical absorption method, the solid sorption method, and the low temperature condensation method. Membrane separation technology is characterized by a small footprint, low energy consumption, easy operation and low pollution, and is considered as the most promising gas separation technology [9]. Amine absorption [10] is the most common industrial technology for capturing CO_2 from smoke flow, but it is limited to low-temperature (40–150 °C) applications, and incurs a considerable cost and requires a high degree of

energy for absorber regeneration, which is vulnerable to equipment corrosion and may produce dangerous waste by-products. Solid physical sorption of microporous and mesoporous materials such as activated carbon, zeolite and carbon fiber can also capture CO_2 at low temperatures, but they are not effective above 300 °C. If the gas can exceed 500 °C, the use of activated carbon and zeolite may require cooling and additional costs [11]. Alkaline metal base chemical sorption at high temperatures can better solve the problem of CO_2 capture under high temperature conditions. CaO-based sorbents, including calcium carbonate, carbide slag and eggshell, show high CO_2 capture ability, stability and durability after a repeated cycle, good wear resistance and mechanical strength, good dynamic characteristics, strong competitive cost and good regeneration. These factors make CaO a good sorbent for capturing CO_2 [12]. The low-temperature condensation method achieves separation of CO_2 from flue gas by liquefaction, and is only applicable to mixed gas with high CO_2 concentration [13]. The main problems are its large system area and high energy consumption.

Compared with other capture methods, including amine absorption [14], absorption of microporous, and mesoporous materials [11], calcium looping for CO_2 capture from the fossil fuel combusiton flue gas by absorption/separation through the use of calcium-based sorbents is regarded as a cheap CO_2 capture technology with large-scale commercial application and high CO_2 capture efficiency [15,16]. Calcium-based sorbents undergo carbonation within the temperature range from 600 to 700 °C, which involves capturing CO_2 from flue gas to generate calcium carbonate ($CaCO_3$). Subsequently, $CaCO_3$ undergoes calcination within the temperature range from 850 to 950 °C, producing a highly concentrated CO_2 flue gas, which can be separated, and calcium-based sorbents can be cycled in the calcium looping process [17,18].

After a limited re-cycle number, the adsorption properties of calcium-based absorbent show a noticeable trend of decay owing to the high-temperature sintering in the calcination process [19–21]. The micropore characteristics as well as particle surface area could be gradually decreased due to the high-temperature sintering behavior in the multiple cyclic calcination process, and then influence the carbonate conversion rate of absorbents. Furthermore, a growth of CaO sub-grain will also decrease the surface reaction and melting of the micro-surface from the fuel or absorber impurities. Therefore, the rate and extent of the gas-solid reaction are reduced [22]. A small amount of water vapor in flue gas plays a certain role in improving sintering. $Ca(OH)_2$ generated by the reaction between water vapor and CaO decomposes into CaO with smaller crystal size during dehydration, which can achieve higher porosity, larger surface area and pore volume, and higher reactivity, and can promote the carbonation reaction [23,24]. CaO mixed with the polystyrene spheres by template synthesis in the desired ration to obtain innovative CaO-based sorbents, has shown a good performance of sintering resistance, too [25,26].

The decay mechanism of cyclic CO_2 capture performance by calcium-based sorbents can be evaluated by its physical and chemical characterizations [27], including XRD test (the components and crystal structure of sorbents), BET test (surface and pore size distribution) and SEM test (the surface microstructure and product characteristics), etc. Scientists have conducted numerous studies to describe the decay mechanism of calcium-based sorbents and proposed the prediction models characterizing the cyclic attenuation characteristics of calcium-based sorbents [28–31], along with the suitable methods or recommended values to determine parameters in the model. However, the precursors of CaO-based sorbents have different solid phases or polymorphs crystal structures. For example, the XRD patterns reveal that calcite belongs to a trigonal symmetry system, and it has a broad particle size distribution; aragonite belongs to an orthorhombic crystal system, and it has needle-like crystal habits; while vaterite belongs to a hexagonal crystal system, and it has no distinct morphology [27]. The critical parameters in the above model should be associated with the physicochemical characterization of sorbents for their different crystal structures.

Therefore, 20-cycle experiments with those three types of calcium-based sorbents for CO_2 capture under the non-isothermal thermogravimetric condition were performed to

explore the the decay characteristics of the best sorption capacity of sorbents in the multi-cycle and calculate the hypothetical carbonation conversion and carbonation conversion for an infinite number of cycles by redefining them based on the physical and chemical characterization results.

2. Experiment

2.1. Preparation of Waste Calcium-Based Sorbents

In order to reduce the cost of calcium-based sorbents, carbide slag and chicken eggshells were used in this study, and analytical reagent (AR)-grade $CaCO_3$ was also used for comparative analysis with carbide slag and chicken eggshells. Carbide slag and chicken eggshells were obtained from a resin manufacturing plant and a cake factory in Guizhou Province, China, respectively. In order to improve the grinding quality of calcium-based sorbents (carbide slag, chicken eggshells, and AR-grade $CaCO_3$), the three calcium-based sorbents were dried in an electric blast drying oven (101-0ASB; Guizhou Hengtai Kelian Co., Ltd., Guiyang, China) at 120 °C for 2 h firstly, and ground and sieved to obtain 150-mesh particles (105 μm). After calcination in a muffle furnace (Smart-1, China) at 700 °C for 20 min, the sorbents were removed cooled in an airtight drying cabinet, and transferred to bottles for storage. The calcined carbide slag, chicken eggshells, and AR-grade $CaCO_3$ sorbent samples were named CS, RES, and APC, respectively.

2.2. Experimental System and Operating Conditions for CO_2 Capture

The experiment was performed on a simultaneous thermogravimetric analyzer (STA) (STA409 PC; NETZSCH, Selb, Germany), as shown in Figure 1. Features of the STA were shown as follows: simultaneous TG and DSC signal measurements; automatic generation of TG/DSC curves; temperature ramp rate: 0.1–50 °C/min; temperature measurement range: from ambient temperature to 1500 °C; reaction atmospheres: oxidizing, reducing, inert, and certain corrosive gases (non-toxic, not highly flammable); maximum sample weight: 18 g; constant-temperature water bath.

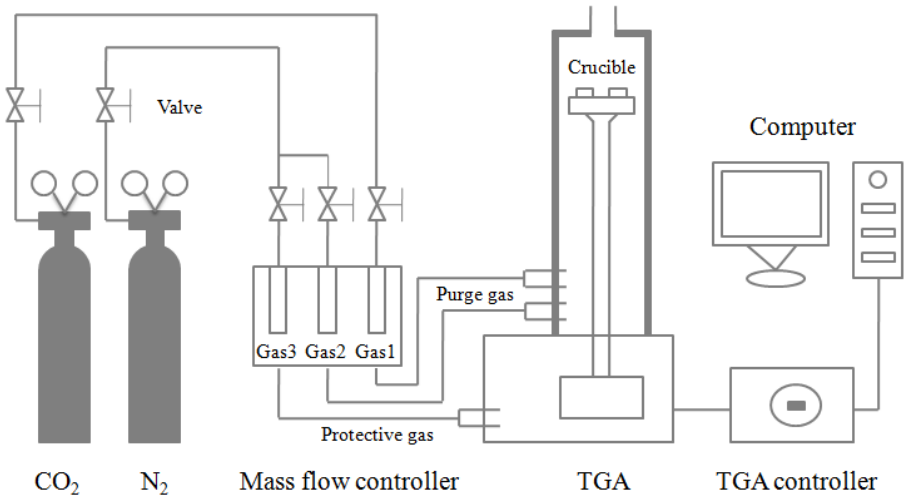

Figure 1. Schematic of STA409 PC.

To control the precision of sample weights, 10 mg of each calcium-based sorbent sample was measured for each experimental run using an electronic analytical balance (BT25S; Sartorius, Gottingen, Germany) with a readability of 0.01 mg.

Table 1 shows the reaction conditions for the cyclic calcination/carbonation experiment. The various steps of the reaction process were as follows. (1) Step 1 (preheating stage): temperature was increased from 30 °C to 600 °C at a heating rate of 5 °C/min in an N_2 atmosphere; this stage is mainly to remove the moisture component of sorbents in long term storage. (2) Step 2 (carbonation stage): CO_2 at a concentration of approximately 30%

was introduced for the simulation of flue gas, and the system was further heated to 750 °C at a rate of 5 °C/min for carbonation; this stage is the process of gaining weight. (3) Step 3 (calcination stage): inflow of CO_2 was stopped, the flow rate of N_2 was kept unchanged, and the temperature was increased to 900 °C at a rate of 5 °C/min for calcination; this stage is the process of losing weight. (4) Step 4 (cooling stage): The flow rate of N_2 was kept unchanged, and the system was cooled to 600 °C at a rate of 5 °C/min; this is the temperature condition for the carbonation reaction again. After the completion of one cycle, the next cycle was performed by repeating Steps 2 to 4.

Table 1. Experimental conditions for cyclic calcination/carbonation.

Step	Temperature Range (°C)	Reaction Gas	Gas Flow Rate (mL/min)	Rate of Temperature Increase (Decrease) (°C/min)	Stage
1	30–600	N_2	50	5	Preheating
2	600–750	N_2	50	5	Carbonation
		CO_2	20		
3	750–900	N_2	50	5	Calcination
4	900–600	N_2	50	5	Cooling
5	Repeat steps 2–4				

2.3. Analysis Methods

To determine the reactivity of calcium-based sorbents during the carbonation stage, the initial mass of each experimental sample, the mass of the sample before and after each carbonation cycle, mass fraction of CaO in the sample, and molar masses of the reaction products were used for the calculation of carbonation conversion (X_N) [32,33], carbonation conversion rate (R_N), amount of CO_2 captured (C_N), and calcination decomposition (Y_N) using Equations (1)–(4) below:

$$X_N = \frac{m_{N,t} - m_{N,s}}{Am_0} \times \frac{M_{CaO}}{M_{CO_2}} \quad (1)$$

where X_N is the carbonation conversion during Cycle N (mol/mol); m_0 is the initial mass of the sorbent (g); A is the mass fraction of CaO in the sorbent; $m_{N,\,t}$ is the mass of the sorbent during Cycle N or at time t (g); $m_{N,s}$ is the initial mass of the sorbent for Cycle N (g); M_{CaO} is the molar mass of CaO (g/mol); and M_{CO2} is the molar mass of CO_2 (g/mol).

$$R_N = \frac{dX_N}{dt} \quad (2)$$

where R_N is the carbonation conversion rate during Cycle N (s-1); t is the reaction time (s).

$$C_N = \frac{m_{N,t} - m_{N,s}}{m_0} \quad (3)$$

where C_N is the amount of CO_2 captured during Cycle N (g/g).

2.4. Characterization of Sorbents

The mass percentage of the main components of the sample was detected by an X-ray Fluorescence (XRF) spectrometer (Netherlands Panaco, Axiosmax wavelength dispersive).The phase composition of the calcium-based sorbent hole was tested by a small-angle X-ray Diffraction (XRD) spectrometer, (German Broker, D8 Advance), and the pore structure and specific surface area of the calcium-based sorbent were tested using the automatic specific surface microvoid analyzer (American Mick, ASAP2460 (M)).

3. Results and Discussion

3.1. Characterization Analysis of Sorbents

Figure 2 shows the XRD pattern of CS, RES, and APC. The CaO diffraction peaks with the same trend appear at 32.39°, 37.54°, 54.03°, 64.30°, and 67.52°. The peak height was the highest at 37.54°, implying that the three sample precursors were fully decomposed into CaO after calcination. The main peak of REG is higher and narrower than that of CS and APC, which means larger grain size according to Debys-Scherer's formula. The quantitative composition analysis of CS and RES was completed by XRF, as shown in Table 2. Because of different precursors, the mass percentage of CaO in the sample was different. APC was the largest while CS was the smallest.

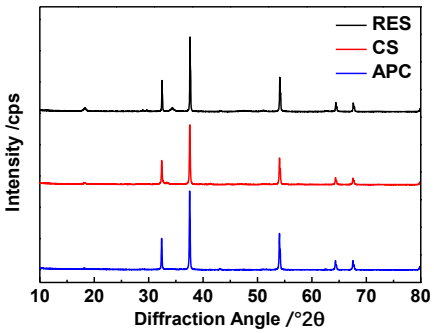

Figure 2. X-ray diffraction results of sorbents.

Table 2. The chemical composition of samples (wt %).

Component Sample	CaO	SiO_2	Al_2O_3	Fe_2O_3	MgO	Other	LOI
CS	73.88	4.6	2.69	0.35	0.015	0.645	17.82
RES	85.15	0.04	0.43	0.12	0.015	1.184	13.061

The N_2 adsorption isotherms of the samples are shown in Figure 3. They were concave in the early stage, linear in the middle stage, and convex in the late stage with the relative pressure p/p°. The isotherm had an obvious inflection point in the low-pressure region. The first layer of adsorption was before the inflection point. As the relative pressure increased, multi-layer adsorption began to occur. The isotherms showed a rapid growth trend until reaching the saturation state when the relative pressure p/p° range was within 0.85 to 1. There was a narrow H_3-type hysteresis loop when the relative pressure p/p° range was within 0.75 to 1, characterized by macroporous channels and micropore dysplasia. Hence, the isotherms were classified as type IIb according to the International Union of Pure and Applied Chemistry physical adsorption [34].

The specific surface area was calculated using the BET method (SBET) according to isotherm type using the N_2 adsorption data. The density functional theory method was applied to obtain the size distribution by solving the generalized adsorption isotherm (GAI) integral equation, which is based on the assumption that the measured isotherm is composed of a large number of single-pore isotherms, and this is how the isotherms are distributed. The total pore volumes V_{total} was calculated according to the adsorbed quantities of N_2 at the relative pressure p/p° of ca. 0.995. The average pore diameter was obtained using $4V_{total}/S_{BET}$. Table 3 shows the highest adsorbed capacity and largest average pore diameter for sample CS, the largest specific surface for sample APC, and the lowest value of three parameters for sample REG. Figure 4 confirms the ordering of the above parameters. Based on pore structure, the samples were mainly composed of mesoporous (2–50 nm) and microporous (>50 nm) structures, and microporosity was scarcely developed. Sample APC had a well-developed mesoporous structure, with a pore diameter around 7–30 nm. The microporous structure was relatively developed for sample

CS, and sample RES showed mesoporous characteristics within a more comprehensive pore diameter range.

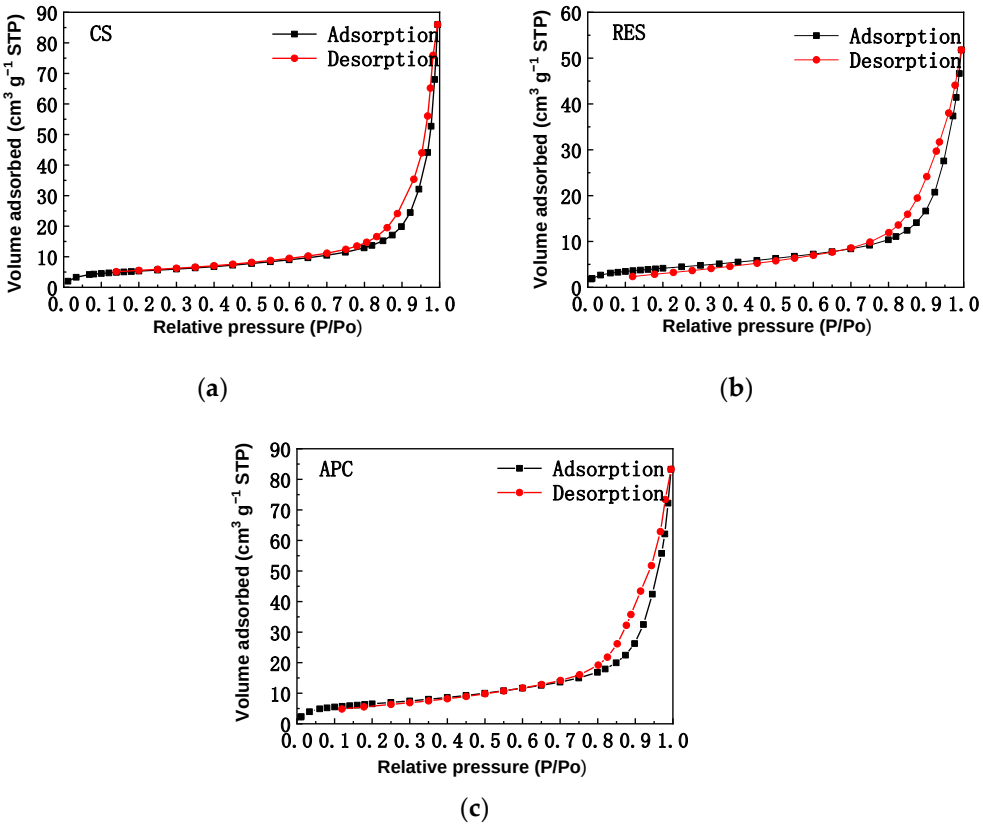

Figure 3. N_2 adsorptions isotherms of samples: (**a**) calcined carbide slag; (**b**) chicken eggshells; (**c**) AR-grade $CaCO_3$.

Table 3. Surface and pore structure statistics of samples measured from N_2 absorption.

Samples	S_{BET} (m^2 g^{-1})	V_{total} (cm^3 g^{-1})	Average Pore Diameter (nm)
CS	18.4321	0.132978	29.0178
RES	15.2060	0.080103	21.0714
APC	23.6375	0.128815	21.7984

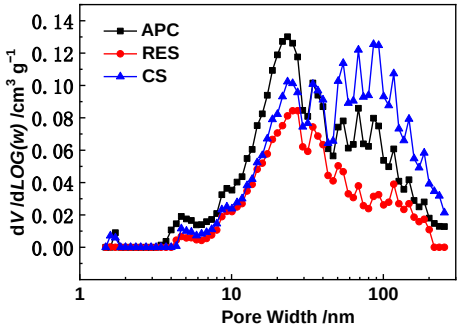

Figure 4. Pore size distribution of samples.

3.2. Influence of Cycle Number on CO_2 Capture Characteristics of Calcium-Based Sorbents

Figure 5 shows the influence of cycle number on the CO_2 capture characteristics of the three sorbents. Figure 5a shows that the carbonation conversion (X_N) of CS and RES exhibited a decreasing trend as cycle number increased. RES exhibited the most significant

decrease in X_N, with X_6 having a value of 0.331 mol/mol, which decreased by 50.68% as compared with X_1. The XN values for CS followed a linear trend of decrease. The average decay of carbonation conversion after each cycle was approximately 0.01 mol/mol. For APC, optimum carbonation conversion and stable reactivity were maintained throughout the 20 cycles. The difference in X_N with CS increased as the cycle number increased. Figure 5b shows the relationship between CO_2 captured (C_N) and cycle number. During the 20 cycles, the C_N value of APC remained higher than that of other sorbents. Except for the first six cycles, the trends of CN for CS and RES were similar. As the cycle number increased, the difference in CN between APC and CS varied within the range of 0.151–0.158 g/g. The differences between APC and RES varied within the scope of 0.313–0.325 g/g.

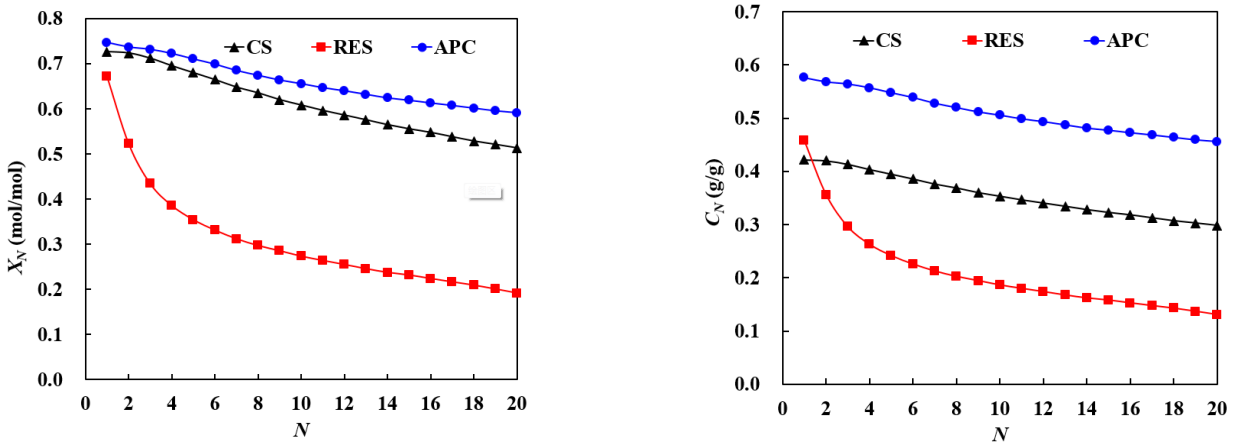

Figure 5. Influence of cycle number on the cyclic CO_2 capture characteristics of calcium-based sorbents: (**a**) relationship between X_N and N; (**b**) relationship between C_N and N.

Furthermore, the influence of cycle number on the CO_2 capture characteristics of CS can be determined from the analysis of Figures 5 and 6. As shown in Figure 5, X_N reached a maximum value of 0.726 mol/mol during Cycle 1 and subsequently decreased as the cycle increased. The value of X_{20} was 0.514 mol/mol, which was 29.28% lower than that of X_1. To further investigate the influence of cycle number on carbonation in CS, the variations in X_N and C_N with reaction time during ten cycles, including Cycles 1 and 20, were analyzed in detail. From Figure 6, it can be seen that the curves shifted toward the right as the cycle number increased, which indicates a decrease in the duration of the rapid chemical reaction-controlled stage. This may be explained by changes in micropore structures on the sorbent surfaces caused by high-temperature sintering. In each cycle, grain growth occurred during carbonation, and grain fragmentation occurred during calcination, which may have influenced the micropore structures and porosity of the sorbent and resulted in a reduction in CO_2 capture activity. Conversion at the same reaction time point decreased as the cycle number increased. At a reaction time of 3 min, the values of X_N and C_N were 0.377 mol/mol and 0.219 g/g during Cycle 1. The corresponding values for Cycle 20 were 0.095 mol/mol and 0.055 g/g, which had decreased by 74.96% compared with Cycle 1. The degrees of carbonation during Cycles 7 to 20 were relatively similar. At a reaction time of 15 min, the values of X_N and C_N were 0.563 mol/mol and 0.327 g/g during Cycle 1. The corresponding values for Cycle 20 were 0.310 mol/mol and 0.180 g/g, which had decreased by 44.94% compared with Cycle 1. Differences in X_N and C_N were significant between adjacent cycles. During the reaction period of 3–15 min, differences in X_N and C_N between adjacent cycles gradually increased with time. They gradually decreased with an increase in the cycle number.

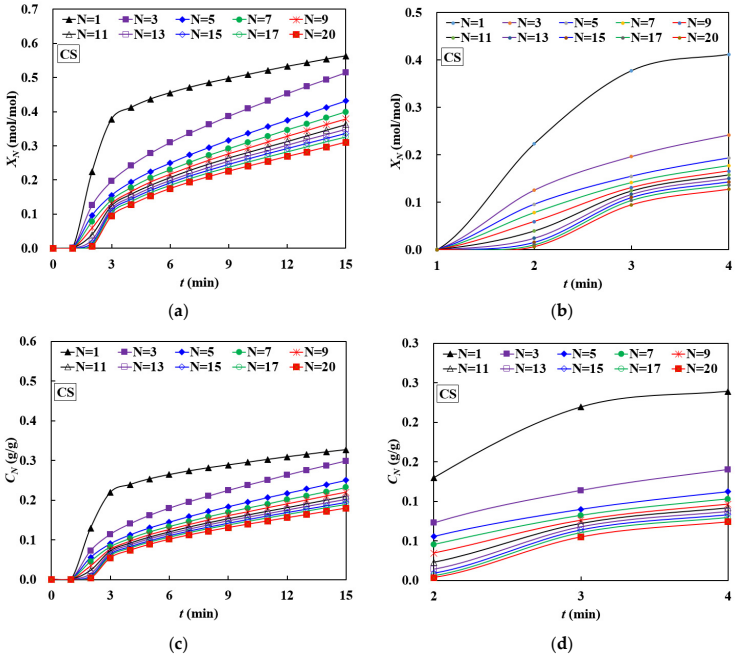

Figure 6. CO_2 capture characteristics of CS during different cycle number: (**a**) relationship between X_N and N; (**b**) zoom of (**a**); (**c**) relationship between C_N and N; (**d**) zoom of (**c**).

From Figure 5, it can be seen that X_1 and X_{20} for RES were 0.672 mol/mol and 0.192 mol/mol, respectively, which indicates a 71.43% decrease from Cycle 1 to Cycle 20. Figure 7 shows that the reactivity of RES was significantly higher during Cycle 1. At a reaction time of 3 min, the values of X_N and C_N were 0.334 mol/mol and 0.223 g/g during Cycle 1; however, the corresponding values for Cycle 3 had decreased considerably to 0.084 mol/mol 0.056 g/g. As the cycle number increased, the degree of carbonation at the same reaction time point decreased gradually. Except for the first two cycles, there were few changes in the X_N values for RES after 3 min of reaction in each cycle.

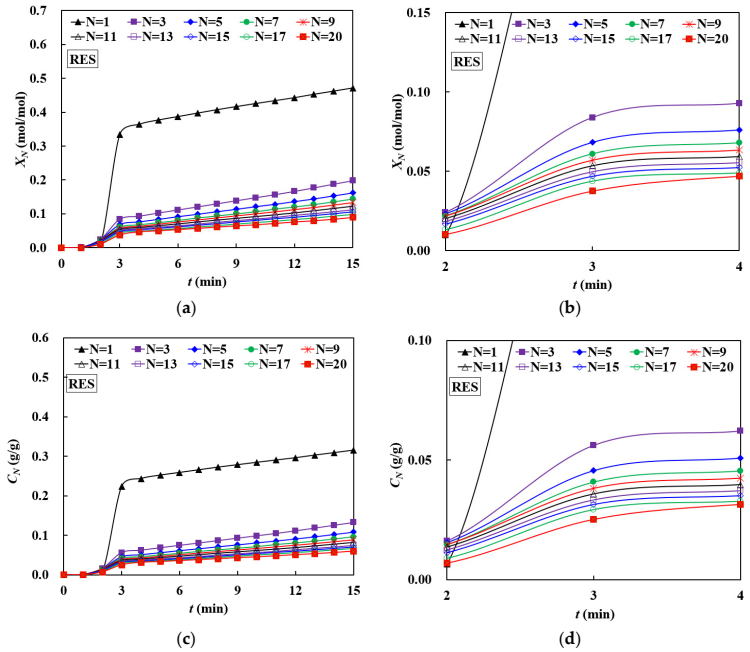

Figure 7. CO_2 capture characteristics of RES during different cycle number: (**a**) relationship between X_N and N; (**b**) zoom of (**a**); (**c**) relationship between C_N and N; (**d**) zoom of (**c**).

As shown in Figure 5, the decay of X_N of APC with an increase in cycle number was less significant than CS and RES. X_N reached a maximum value of 0.747 mol/mol during Cycle 1 and subsequently decreased continuously to 0.591 mol/mol after Cycle 20; a 20.87% decrease compared with Cycle 1. From Figure 8, it can be seen that the degrees of carbonation at a reaction time of 3 min were similar among the various cycles. This may be because the rapid chemical reaction-controlled stage was mainly influenced by reaction temperature and external surface area, which limited the influence of sintering-induced micropore structure changes after multiple cycles on the degree of carbonation in APC during this stage. The X_N values after 3 min of reaction for the various cycles exhibited significant changes with an increase in reaction time. At a reaction time of 15 min, the values of X_N and C_N were 0.492 mol/mol and 0.377 g/g during Cycle 1; the corresponding values for Cycle 20 were 0.378 mol/mol and 0.292 g/g, and the difference between the maximum and minimum X_N values and difference between the maximum and minimum C_N values for APC were 0.156 mol/mol and 0.120 g/g, respectively.

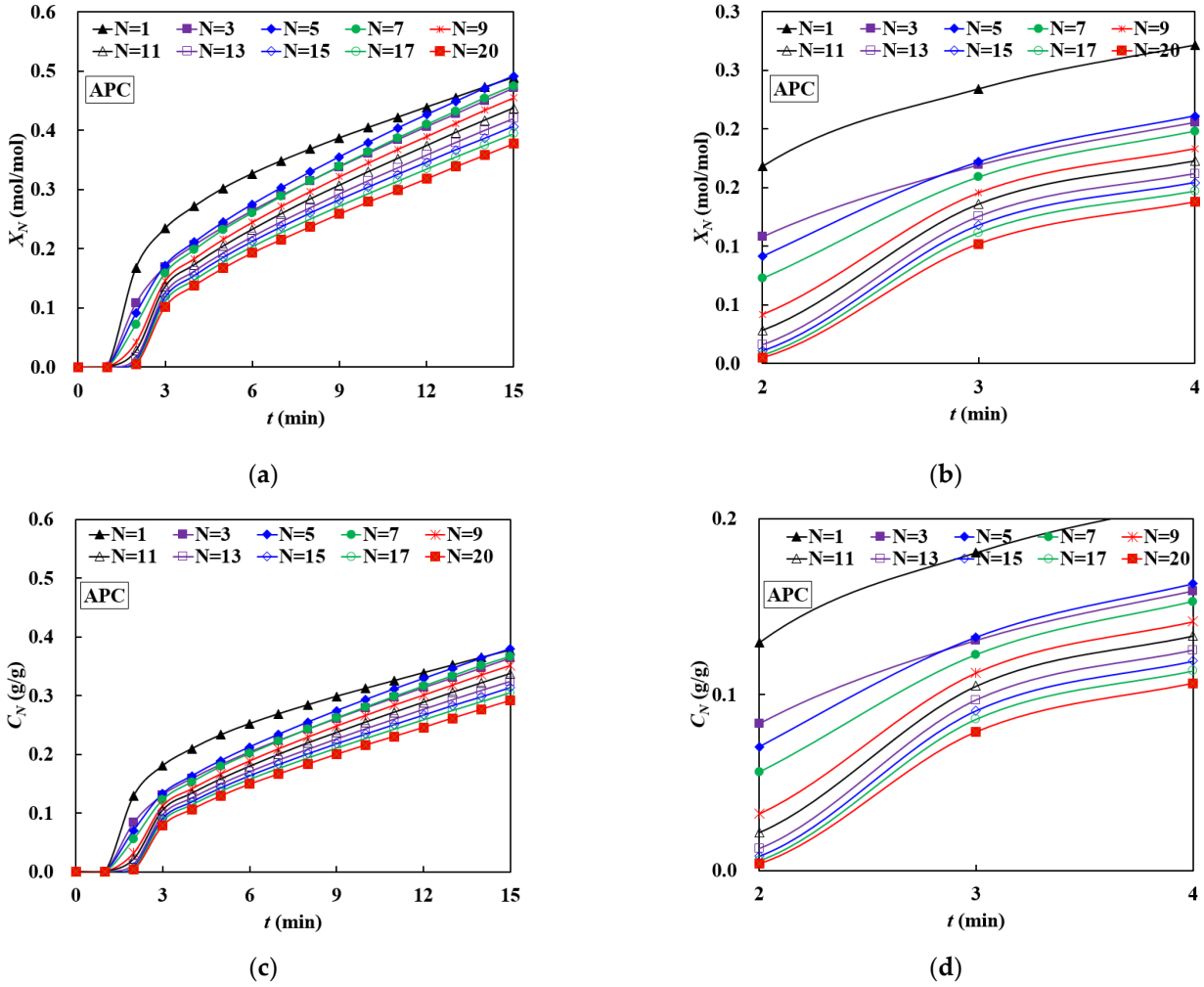

Figure 8. CO_2 capture characteristics of APC during different cycle number: (**a**) relationship between X_N and N; (**b**) zoom of (**a**); (**c**) relationship between C_N and N; (**d**) zoom of (**c**).

3.3. Influence of Reaction Time on CO_2 Capture Characteristics of Calcium-Based Sorbents

Figure 9 shows the variation in X_N and R_N during Cycles 1 and 20 (X_1, R_1, X_{20}, and R_{20}) of the three calcium-based sorbents with reaction time.

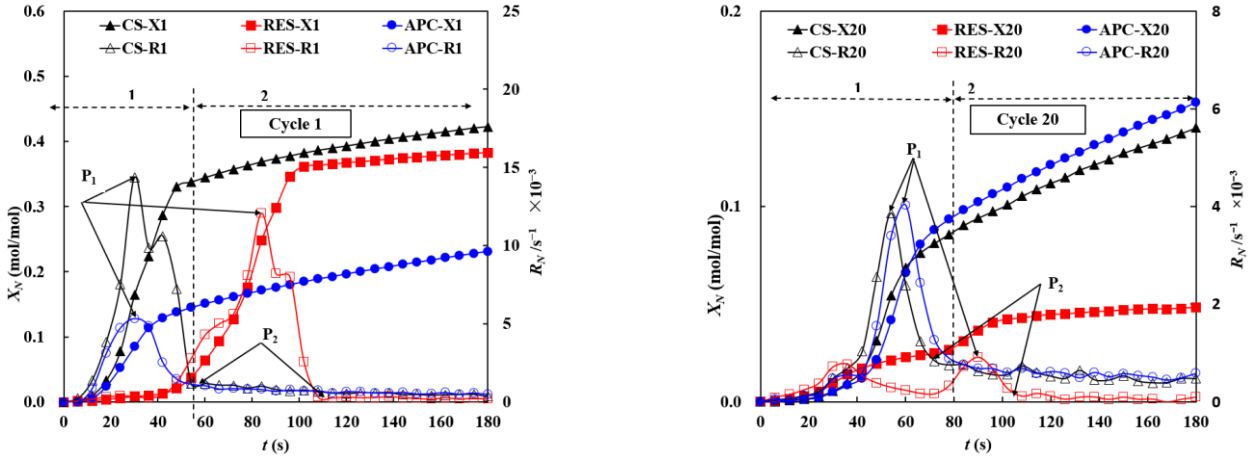

(**a**) (**b**)

Figure 9. Influence of reaction time on the cyclic CO_2 capture characteristics of calcium-based sorbents: (**a**) relationship between X_N and N; (**b**) relationship between R_N and N.

From Figure 9, it can be seen that the variations in X_1 for CS and RES with carbonation time were consistent, exhibiting a rapid increase during the initial stage and a gradual increase during the later stage. P_1 and P_2 on the R_1 curves for the three sorbents represent the peak carbonation conversion rate and inflection point, respectively. Parameters corresponding to P_1 can be calculated from the first and second derivatives of the carbonation curves. For CS, P_1 and P_2 occurred at approximately 30 s and 52 s, respectively; the corresponding timings for RES were 84 s and 108 s, with the significant lag possibly caused by the presence of the eggshell membrane in RES. The period between t = 0 and the time point at which P_2 occurred represents the rapid chemical reaction-controlled stage. The CO_2 captured by CS and RES during this stage accounts for 46.45% and 54.06% of the total CO_2 captured. It was observed that CS exhibited better CO_2 capture ability and achieved a shorter reaction time. This may be because carbide slag mainly consists of Ca $(OH)_2$, which underwent dehydration during the calcination process to form CaO.

Consequently, hydraulic fracturing occurred, leading to increased surface area and porosity in the sorbent and an enhanced ability to react with CO_2 [35]. For APC, the time at which R_1 peaked was close to that of CS, but the peak value of 5.34×10^{-3} s^{-1} was much lower than the peak value of 14.37×10^{-3} s^{-1}. The amount of CO_2 captured during the rapid chemical reaction-controlled stage accounted for 19.38% of the total CO_2 captured, which is lower than the corresponding proportions for CS and RES. One possible reason for this is that during the rapid chemical reaction-controlled stage of the carbonation reaction, it was mainly controlled by the total specific surface area of sorbent, which consisted of the external and micropore surface area of the sorbent particles. After the maximum carbonation conversion rate had been reached at P_1, R_1 started to decrease with an increase in the thickness of the $CaCO_3$ product layer formed on the external surfaces and pores of the sorbent through reaction with CO_2. Subsequently, the reaction entered the slow diffusion-controlled stage at P_2, during which R_1 was mainly determined by the diffusion resistance encountered by CO_2 when passing through the $CaCO_3$ product layer before further reaction with CaO within the internal pores of the sorbent.

During Cycle 20, carbonation conversion and carbonation conversion rates were significantly lower compared with those for Cycle 1. For CS, P_1 and P_2 occurred at approximately 54 s and 80 s, respectively, considerably later than that of Cycle 1. In addition, the proportion of total CO_2 captured contributed by CO_2 captured during the rapid chemical reaction-controlled stage also decreased significantly to 16.70%. For RES, the peak R_{20} value at 84 s was relatively indistinct, which indicates the occurrence of severe sintering-induced pore collapse and blockage in the sorbent. Reductions in the rate and degree of carbonation

may be explained by the decrease in specific surface area of the sorbent after multiple cycles, as high-temperature sintering led to decreased grain growth in the micropores [36]. For APC, R_{20} peaked at approximately 60 s with a value of 4.02×10^{-3} s^{-1}, slightly higher than the value of 3.86×10^{-3} s^{-1} for CS. It merely decreased by 1.32×10^{-3} s^{-1} compared with the peak R_1 value. This shows that APC was influenced by high-temperature sintering to a smaller extent.

3.4. Characteristics of Decay of Carbonation Reactivity

During the rapid chemical reaction-controlled stage, a $CaCO_3$ product layer with a thickness of approximately 0.2 µm was formed on the grain surfaces of CaO [37], constituting the main resistance to CO_2 diffusion during the slow diffusion-controlled stage. Pores within CaO can be classified as micropores if they have a diameter of ≤0.2 µm and macropores if they have a diameter of >0.2 µm. Micropores allow the carbonation reaction to remain in the rapid chemical reaction-controlled stage. By contrast, macropores promote an increase in the thickness of the $CaCO_3$ product layer, which drives the carbonation reaction toward the slow diffusion-controlled stage. During multiple cycles, carbonation reactivity in the sorbent is regained through calcination. However, prolonged high-temperature sintering effects also result in the fusion of grains on CaO surfaces. This causes a gradual decrease in micropores and a gradual increase in the number of macropores in CaO as the cycle increases, reducing sorbent activity and carbonation conversion. To describe the relationship between carbonation conversion in calcium-based sorbents and cycle number, researchers have proposed several prediction models for the characterization of cyclic carbonation reactivity decay in calcium-based sorbents, as shown in Equations (4) [28], (5) [29], (6) [30] and (7) [31].

$$X_N = f_m^N(1 - f_w) + f_w \tag{4}$$

$$X_N = \frac{1}{1 + kN} \tag{5}$$

$$X_N = \frac{1}{\frac{1}{1 - X_r} + kN} + X_r \tag{6}$$

$$X_N = \frac{X_1}{\frac{X_1}{X_1 - X_r} + k(N - 1)} + X_r \tag{7}$$

where X_N is the carbonation conversion rate during Cycle N (mol/mol); N is the cycle number; f_m and k are the deactivation constants; f_w and X_r are the carbonation conversion values for an infinite number of cycles (mol/mol); and X_1 is the carbonation conversion value during Cycle 1.

Abanades and Alvarez [28] regarded f_m and f_w as fitting parameters associated with micropores and macropores, respectively, with values of 0.77 and 0.17. Wang and Anthony contended that Equation (4) was only applicable to cycle numbers < 20 and proposed a simplified single-parameter equation (see Equation (5)) with a k value of 0.06, on the basis that the reaction conditions do not primarily determine the decay of the reactivity of calcium-based sorbents; however, Equation (5) implies that carbonation conversion will approach 0 when cycle number approaches infinity, which is not consistent with reality. Bouquet et al. [38] contended that carbonation during the cyclic reaction occurs on the surfaces of CaO micrograins and that carbonation conversion is proportional to the number of micrograins. During the calcination process, a particular portion of micrograins loses their reactivity because of sintering, which leads to a reduction in the effective specific surface area of the sorbent grains and a consequent decay of reactivity. In successive cyclic reactions, the carbonation conversion of a sorbent is proportional to the effective specific surface area of the sorbent grains during the cycle. When cycle number becomes large, the effective specific surface area of the sorbent is essentially the external surface area of the sorbent grains, as all micrograins would have fused because of sintering. Ultimately,

the carbonation conversion will gradually converge to a constant, expressed as f_w in Equation (5) and X_r in Equations (6) and (8).

Equation (6) is a semi-empirical equation proposed by Grasa and Abanades [30] following the investigation of a long series of carbonation/calcination cycles performed using limestone. For most limestone sorbents, values of 0.075 and 0.52 are used for k and X_r, respectively. As sintering begins during the calcination stage of Cycle 1, a hypothetical carbonation conversion rate X_0 can be defined. By setting N as 0 and assuming that all CaO micrograins participate in the reaction, the value of $X_0 = 1$, as given by Equations (5) and (6). Subsequently, Valverde [31] proposed Equation (7) by incorporating the carbonation conversion of Cycle 1 (X_1).

To use the models described above in predicting the decay characteristics of the calcium-based sorbents, the carbonation conversion rates for an infinite number of cycles based on the actual conditions of the various calcium-based sorbents were calculated as follows:

$$X_r = X_0 \frac{A_r}{A_0} \tag{8}$$

where X_r is the carbonation conversion for an infinite number of cycles (mol/mol); X_0 is the hypothetical carbonation conversion (mol/mol); A_0 is the hypothetical specific surface area of the sorbent (m^2/kg), and A_r is the specific surface area of the sorbent for an infinite number of cycles (m^2/kg).

Based on the variation patterns of carbonation conversion for 20 cycles of the various sorbents, the Cycle 0 hypothetical carbonation conversion values of CS, RES, and APC were calculated as 0.7535 mol/mol (correlation coefficient R = 0.9989), 0.7208 mol/mol (R = 0.9871), and 0.7652 mol/mol (R = 0.9986) by polynomial extrapolation, respectively. Using the diameters of the initial CaO and CaO generated from calcination, the values of 9.1 m^2/kg and 1.6 m^2/kg were calculated for A_0 and A_r, respectively [38]. By substituting these values into Equation (8), the carbonation conversion values of CS, RES, and APC for an infinite number of cycles were calculated as 0.1325 mol/mol, 0.1267 mol/mol, and 0.1345 mol/mol, respectively.

Table 4 shows the fitted parameter values for the various prediction models and the corresponding correlation coefficients when the models were fitted to the curves in Figure 5.

Table 4. Parameter fitting for models of carbonation reactivity decay.

Model	Coefficient	CS	RES	APC
$X_N = f_m^N(1 - f_w) + f_w$	f_m	0.9462	0.7953	0.9563
	f_w	0.1325	0.1267	0.1345
	R	0.9976	0.9872	0.9983
$X_N = \frac{1}{1+kN}$	k	0.0633	0.3117	0.0491
	R	0.9917	0.9928	0.9963
$X_N = \frac{1}{\frac{1}{1-X_r}+kN} + X_r$	X_r	0.1325	0.1267	0.1345
	k	0.0977	0.5661	0.0742
	R	0.9857	0.9765	0.9934
$X_N = \frac{X_1}{\frac{X_1}{X_1-X_r}+k(N-1)} + X_r$	X_r	0.1325	0.1267	0.1345
	X_1	0.7264	0.6719	0.7471
	k	0.0343	0.3492	0.0237
	R	0.9983	0.9966	0.9976

Table 4 shows that the highest correlation coefficients were obtained with Equation (8). Figure 10 shows the calculated carbonation conversion values for CS, RES, and APC using Equation (8) and the corresponding experimental values. With an increase in cycle

number, the goodness of fit between the calculated and experimental values increased, demonstrating the feasibility of using the model to predict the decay characteristics of calcium-based sorbents. The predicted carbonation conversion values after 100 cycles for CS, RES, and APC were 0.2898 mol/mol, 0.1455 mol/mol, and 0.3438 mol/mol, respectively. These prediction values are similar to those found by Li [39] (the carbonation conversion of $CaCO_3$ remain as high as 0.35 mol/mol after 100 cycles).

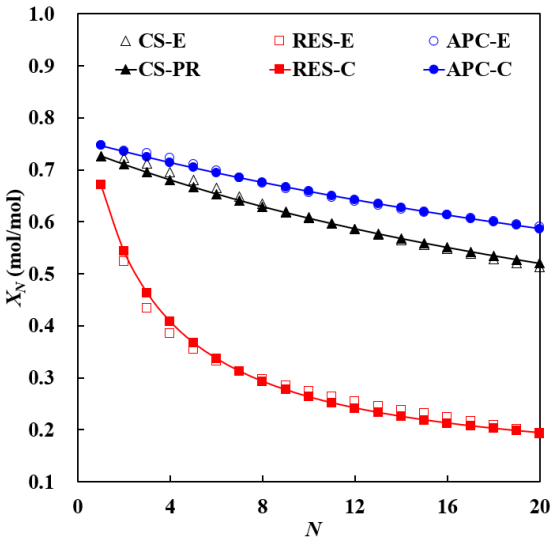

Figure 10. Characteristics of decay of carbonation reactivity.

4. Conclusions

The decay of CO_2 uptake performance in 20 cycles of three calcined sorbents (carbide slag, chicken eggshells, and pure $CaCO_3$ sorbent) were studied by using TGA analysis, and the samples at each stage were tested by XRF, XRD and and N_2 adsorption. The experimental and calculation results have shown that the carbonation conversion of all samples exhibited a decreasing trend as the cycle number increased. RES exhibited the most significant rate of decrease (over 50% compared with Cycle 1) due to high temperature sintering after 6 cycles. CS exhibited a flat linear decline trend, the average decay of carbonation conversion after each cycle was approximately 0.01 mol/mol because CS mainly consists of $Ca(OH)_2$, which underwent dehydration during the calcination process to form CaO. Carbonation conversion of APC remained higher than that of other sorbents. The specific surface area of the samples was used to calculate carbonation conversion for an infinite number of cycles, and the carbonation conversion rates of CS, RES, and APC were estimated to decrease to 0.2898, 0.1455, and 0.3438 mol/mol, respectively, after 100 cycles.

Author Contributions: Conceptualization, Z.Z. and D.G.; methodology, D.G.; software, T.Z.; validation, D.G. and T.Z.; formal analysis, D.G.; investigation, D.G. and T.Z.; resources, D.G.; data curation, D.G. and T.Z.; writing—original draft preparation, D.G.; writing—review and editing, D.G.; visualization, D.G.; supervision, Z.Z.; project administration, Z.Z.; funding acquisition, D.G. All authors have read and agreed to the published version of the manuscript.

Funding: This research was funded by Guizhou Provincial Natural Science Foundation of China (Grant No. [2019] 1059) and Guizhou Provincial Science and Technology Program of China (Grant No. [2022] general 018).

Institutional Review Board Statement: Not applicable.

Informed Consent Statement: Not applicable.

Data Availability Statement: Not applicable.

Conflicts of Interest: The authors declare no conflict of interest.

References

1. Yu, B.Y.; Zhao, G.P.; An, R.Y.; Chen, J.M.; Tan, J.X.; Li, X.Y. Research on China's CO_2 emission pathway under carbon neutral target. *J. Beijing Inst. Technol.* **2021**, *23*, 17–24.
2. Salaudeen, S.A.; Acharya, B.; Dutta, A. CaO-based CO_2 sorbents: A review on screening, enhancement, cyclic stability, regeneration and kinetics modelling. *J. CO_2 Util.* **2018**, *23*, 179–199. [CrossRef]
3. Mukherjee, S.; Bandyopadhyay, S.S.; Samanta, A.N. Experimental measurements and modelling of CO_2 solubility in aqueous mixtures of benzylamine and N-(2-aminoethyl) ethanolamine. *Asia Pac. J. Chem. Eng.* **2018**, *13*, e2264. [CrossRef]
4. Zhang, Z.; Wang, Y.; Zhu, L.; Li, J.; Wang, F.; Yu, G. Effects of coal ash on iron-based oxygen carrier in chemical-looping combustion using three different rank coals as fuel. *Asia Pac. J. Chem. Eng.* **2019**, *14*, e2313. [CrossRef]
5. Habib, M.A.; Badr, H.M.; Ahmed, S.F.; Ben-Mansour, R.; Mezghani, K.; Imashuku, S. A review of recent developments in carbon capture utilizing oxy-fuel combustion in conventional and ion transport membrane systems. *Int. J. Energy Res.* **2011**, *35*, 741–764. [CrossRef]
6. Zhao, N.; You, F. Can renewable generation, energy storage and energy efficient technologies enable carbon neutral energy transition? *Appl. Energy* **2020**, *79*, 115889. [CrossRef]
7. Cai, N.S.; Fang, F.; Li, Z.S. Research and Development on cyclic calcination/carbonation reaction with Ca-based sorbents to CO_2 capture from flue gases. *Proc. Chin. Soc. Electr. Eng.* **2010**, *30*, 35–43.
8. Cheng, Y.H.; Ershun, D.; Tian, X.; Zhang, N.; Kang, C.Q. Carbon capture power plants in power systems: Review and latest research trends. *Glob. Energy Interconnect.* **2020**, *3*, 339–350.
9. Koros, W.J.; Ryan, P.L. Water and beyond: Expanding the spectrum of large-scale energy efficient separation processes. *AIChE J.* **2012**, *58*, 2624–2633. [CrossRef]
10. Moioli, S.; Pellegrini, L.A.; Ho, M.T.; Wiley, D.E. A comparison between amino acid based solvent and traditional amine solvent processes for CO_2 removal. *Chem. Eng. Res. Des.* **2019**, *146*, 509–517. [CrossRef]
11. Kotyczka-Moranska, M.; Tomaszewicz, G.; Labojko, G. Comparison of different methods for enhancing CO_2 capture by CaO-based sorbents, review. *Physicochem. Probl. Miner. Process.* **2012**, *48*, 77–90.
12. Kumar, S.; Saxena, S.K. A comparative study of CO_2 sorption properties for different oxides. *Mater. Renew. Sustain. Energy* **2014**, *3*, 30. [CrossRef]
13. Tian, H.; Sun, R.; Song, C.F.; Deng, S.; Shi, L.F.; Kang, K.; Shu, G.Q. Performance optimization of novel hybrid cryogenic CO_2 capture process with membrane separation. *Chem. Ind. Eng. Prog.* **2010**, *39*, 2884–2892.
14. Moioli, S.; Pellegrini, L.A. Modeling the methyldiethanolamine-piperazine scrubbing system for CO_2 removal: Thermodynamic analysis. *Front. Chem. Sci. Eng.* **2016**, *10*, 162–175. [CrossRef]
15. Tang, S.; Zhu, L.; Fan, J.M.; Jiang, P. Research progress in modified Ca-based sorbents for cyclic CO_2 capture. *Mod. Chem. Ind.* **2015**, *35*, 44–48.
16. Abanades, J.C.; Grasa, G.; Alonso, M. Cost structure of a post combustion CO_2 capture system using CaO. *Environ. Sci. Technol.* **2007**, *411*, 5523–5527. [CrossRef]
17. Champagne, S.; Lu, D.Y.; MacChi, A.; Symonds, R.T.; Anthony, E.J. Influence of steam injection during calcination on the reactivity of CaO-based sorbent for carbon capture. *Ind. Eng. Chem. Res.* **2013**, *52*, 2241–2246. [CrossRef]
18. Materic, V.; Hyland, M.; Jones, M.I.; Holt, R. Investigation of the friability of Calooping sorbents during and after hydration based reactivation. *Fuel* **2014**, *127*, 70–77. [CrossRef]
19. Blamey, J.; Anthony, E.J.; Wang, J.; Fennell, P.S. The calcium looping cycle for large-scale CO_2 capture. *Prog. Energy Combust. Sci.* **2010**, *36*, 260–279. [CrossRef]
20. Feng, Z.X.; Zheng, Y.; Zhang, L.; Zheng, C.G. Research on high temperature sintering behavior of CaO sorbent used in multi-cyclic CO_2 Capturing. *J. Eng. Thermophys.* **2009**, *30*, 537–539.
21. Manovic, V.; Charland, J.P.; Blamey, J.; Fennell, P.S.; Lu, D.Y.; Anthony, E.J. Influence of calcination conditions on carrying capacity of CaO-based sorbent in CO_2 looping cycles. *Fuel* **2009**, *88*, 1893–1900. [CrossRef]
22. Wang, C.B.; Zhou, X.; Zhang, B.; Bai, Y.F. Effect of sintering on the limestone calcination/carbonation looping cycle for CO_2 capture. *Proc. Chin. Soc. Electr. Eng.* **2014**, *34*, 6271–6278.
23. Coppola, A.; Palladino, L.; Montagnaro, F. Reactivation by Steam Hydration of Sorbents for Fluidized-Bed Calcium Looping. *Energy Fuels* **2015**, *29*, 4436–4446. [CrossRef]
24. Zhang, L.; Zhang, B.; Yang, Z.; Guo, M. The role of water on the performance of calcium oxide-Based sorbents for carbon dioxide capture: A review. *Energy Technol.* **2015**, *3*, 10–19. [CrossRef]
25. Sotenko, M.; Fern'andez, J.; Hu, G.; Derevschikov, V.; Lysikov, A.; Parkhomchuk, E.; Semeykina, V.; Okunev, A.; Rebrov, E.V. Performance of novel CaO-based sorbents in high temperature CO_2 capture under RF heating. *Chem. Eng. Process. Process Intensif.* **2017**, *122*, 487–492. [CrossRef]
26. Bazaikin, Y.V.; Malkovich, E.G.; Prokhorov, D.I.; Derevschikov, V.S. Detailed modeling of sorptive and textural properties of CaO-based sorbents with various porous structures. *Sep. Purif. Technol.* **2021**, *255*, 117746. [CrossRef]
27. Olivares-Marín, M.; Cuerda-Correa, E.M.; Nieto-Sánchez, A.; García, S.; Pevida, C.; Román, S. Influence of morphology, porosity and crystal structure of $CaCO_3$ precursors on the CO_2 capture performance of CaO-derived sorbents. *Chem. Eng. J.* **2013**, *217*, 71–81. [CrossRef]
28. Abanades, J.C.; Alvarez, D. Conversion limits in the reaction of CO_2 with lime. *Energy Fuels* **2003**, *17*, 308–315. [CrossRef]

29. Wang, J.S.; Anthony, E.J. On the decay behavior of the CO_2 absorption capacity of CaO-based sorbets. *Ind. Eng. Chem. Res.* **2005**, *44*, 627–629. [CrossRef]
30. Grasa, G.S.; Abanades, J.C. CO_2 capture capacity of CaO in long series of carbonation/calcination cycles. *Ind. Eng. Chem. Res.* **2006**, *45*, 8846–8851. [CrossRef]
31. Valverde, J.M. A model on the CaO multicyclic conversion in the Ca-looping process. *Chem. Eng. J.* **2013**, *228*, 1195–1206. [CrossRef]
32. Yancheshmeh, M.S.; Radfarnia, H.R.; Iliuta, M.C. Influence of steam addition during carbonation or calcination on the CO_2 capture performance of $Ca_9Al_{16}O_{18}$-CaO sorbent. *J. Nat. Gas Sci. Eng.* **2016**, *36*, 1062–1069. [CrossRef]
33. Rong, N.; Wang, Q.; Fang, M.; Cheng, L.; Luo, Z.; Cen, K. Steam hydration reactivation of CaO-based sorbent in cyclic carbonation/calcination for CO_2 capture. *Energy Fuels* **2013**, *27*, 5332–5340. [CrossRef]
34. Rouqueról, J.; Avnir, D.; Fairbridge, C.W.; Everett, D.H.; Haynes, J.M.; Pernicone, N.; Ramsay, J.D.F.; Sing, K.S.W.; Unger, K.K. Recommendations for the characterization of porous solids (Technical Report). *Pure Appl. Chem.* **1994**, *66*, 1739–1758. [CrossRef]
35. Li, C.C.; Cheng, J.Y.; Liu, W.H.; Huang, C.M.; Hsu, H.W.; Lin, H.P. Enhancement in cyclic stability of the CO_2 adsorption capacity of CaO-based sorbents by hydration for the calcium looping cycle. *J. Taiwan Inst. Chem. Eng.* **2014**, *45*, 227–232. [CrossRef]
36. Feng, B.; An, H.; Tan, E. Screening of CO_2 adsorbing materials for zero emission power generation systems. *Energy Fuels* **2007**, *21*, 426–434. [CrossRef]
37. Mess, D.; Sarofim, A.F.; Longwell, J.P. Product layer diffusion during the reaction of calcium oxide with carbon dioxide. *Energy Fuels* **1999**, *13*, 999–1005. [CrossRef]
38. Bouquet, E.; Leyssens, G.; Schönnenbeck, C.; Gilot, P. The decrease of carbonation efficiency of CaO along calcination–carbonation cycles: Experiments and modelling. *Chem. Eng. Sci.* **2009**, *64*, 2136–2146. [CrossRef]
39. Li, Y.J.; Zhao, C.S.; Chen, H.C.; Duan, L.B.; Chen, X.P. Cyclic CO_2 capture behavior of KMnO4-doped CaO-based sorbent. *Fuel* **2010**, *89*, 642–649. [CrossRef]